

**Eigen microstates in self-organized criticality**Yongwen Zhang <sup>\*</sup>*Faculty of Science, Kunming University of Science and Technology, Kunming 650500, China*Maixin Liu, Gaoke Hu , Teng Liu , and Xiaosong Chen <sup>†</sup>*School of Systems Science, Beijing Normal University, Beijing 100875, China*

(Received 29 December 2023; accepted 20 March 2024; published 11 April 2024)

We employ the eigen microstates approach to explore the self-organized criticality (SOC) in two celebrated sandpile models, namely the BTW model and the Manna model. In both models, phase transitions from the absorbing state to the critical state can be understood by the emergence of dominant eigen microstates with significantly increased weights. Spatial eigen microstates of avalanches can be uniformly characterized by a linear system size rescaling. The first temporal eigen microstates reveal scaling relations in both models. Furthermore, by finite-size scaling analysis of the first eigen microstates, we numerically estimate critical exponents, i.e.,  $\sqrt{\sigma_0 w_1}/\tilde{v}_1 \propto L^D$  and  $\tilde{v}_1 \propto L^{D(1-\tau_s)/2}$ . Our findings could provide profound insights into eigen microstates of the universality and phase transition in nonequilibrium complex systems governed by self-organized criticality.

DOI: [10.1103/PhysRevE.109.044130](https://doi.org/10.1103/PhysRevE.109.044130)**I. INTRODUCTION**

Phase transitions and critical phenomena play pivotal roles in understanding complex systems. Classical models, such as the Ising model and percolation model [1], adeptly capture the continuous phase transition properties. In the Ising model, approaching a critical temperature leads to power-law behaviors in thermodynamic quantities like magnetization and susceptibility, with universal critical exponents which are independent microscopic details [1]. However, the applicability of the Ising model to understand critical phenomena in complex systems is constrained by its requirement for thermodynamic equilibrium, a condition seldom met by real complex systems, which predominantly exist in nonequilibrium states.

In 1987, Bak, Tang, and Wiesenfeld (BTW) established the concept of self-organized criticality (SOC) by introducing the BTW sandpile model [2]. Within this model, power-law behaviors were identified in the size of avalanches, with potential implications for understanding phenomena in the real world. For instance, earthquake energy release follows a power-law distribution [3], rainfall exhibits continuous phase transitions [4], and the waiting time statistics of various natural records mirror the sandpile model's behavior [5–8].

The BTW model illustrates the spontaneous evolution of a nonequilibrium system toward a critical state marked by slow driving energy and rapid energy dissipation [9]. A continuous phase transition between an absorbing state and an active phase is a distinctive feature of the sandpile model [10–12]. The BTW model, characterized by an Abelian group structure, draws an analogy with the Abelian Manna model, which incorporates random relaxation rules [13,14]. Zhang also

proposed another SOC model involving continuous energy [15]. Experimental validation of SOC behavior was demonstrated through a rice pile experiment [16,17]. The universality class of various SOC models, including both the BTW and Manna models, has been reported as identical [18,19]. Nevertheless, there exists some contention regarding the assertion that they might belong to distinct universality classes [20,21].

In this paper, we introduce the concept of eigen microstates of the statistical ensemble to explore the critical behaviors of sandpile models. The critical state can be delineated by the condensed eigen microstates, characterized by the emergence of a substantial weight factor. This characterization finds support in the Ising model [22–24] and collective motion [25]. Our proposed methodology enables the identification of phase transitions and universality classes in nonequilibrium systems without requiring knowledge of the order parameter.

In the subsequent section, we elucidate the definition of SOC sandpile models and articulate the concept of the eigen microstates within the statistical ensemble for the system. Section III provides a detailed exposition of the simulations conducted on SOC sandpile models, along with the presentation of results pertaining to their eigen microstates, analyzed through finite-size scaling. Conclusive remarks are then drawn in Sec. IV.

**II. MODEL DEFINITION AND METHODS****A. The SOC sandpile models**

We explore two models exemplifying SOC: the BTW model and the Abelian Manna model. For the BTW model, we examine a square lattice with  $N = L^2$  sites, where  $L$  represents the system's size. The initial state involves a random distribution of nonnegative integer heights  $z$  for sites, with a

<sup>\*</sup>zhangyongwen77@gmail.com<sup>†</sup>chenxs@bnu.edu.cn

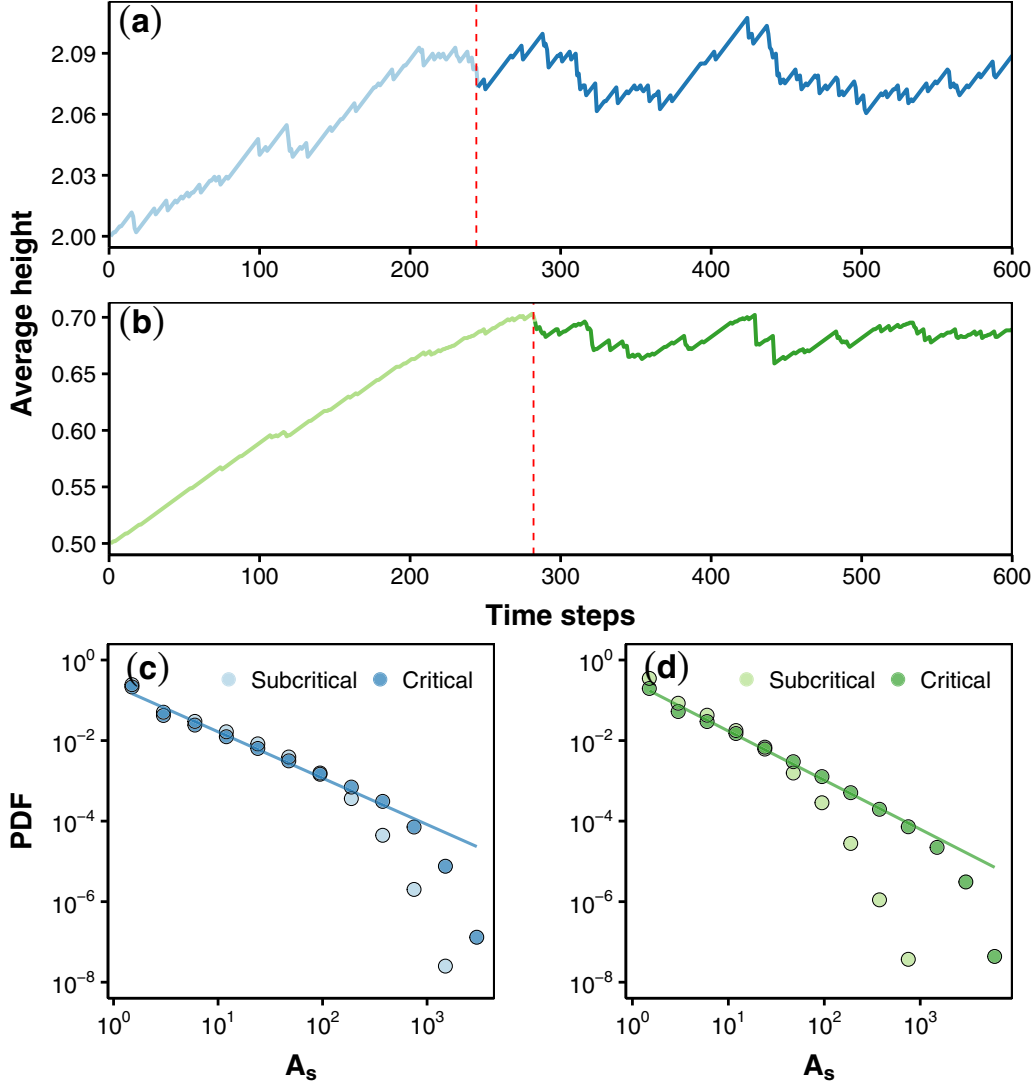


FIG. 1. Evolution of the average height of the sandpile from the absorbing state to the critical state for (a) the BTW model and (b) the Manna model with  $L = 32$ . The system reaches the critical state after the time step indicated by the red dashed line. PDFs of the avalanche size in subcritical and critical states for (c) the BTW model and (d) the Manna model. The lines represent fitted lines with slopes of  $-1.1 \pm 0.07$  in (c) and  $-1.17 \pm 0.04$  in (d), respectively.

given average height. The system undergoes driving forces by adding a grain to a randomly chosen site  $i$ , resulting in an increase in height  $z_i \rightarrow z_i + 1$ . When  $z_i \geq z_0$  (where  $z_0 = 4$  is a predefined threshold height), the site becomes unstable and topples (relaxes) as  $z_i \rightarrow z_i - 4$ . Furthermore, each nearest neighboring site  $j$  gains one grain, leading to  $z_j \rightarrow z_j + 1$ . Toppling may induce instability in neighboring sites, triggering a cascade of toppling until stability is restored, with grains dissipating from the open boundary. This entire toppling process constitutes an avalanche. New grains are added for the next time step until the last avalanche concludes. Over multiple time steps, the system reaches the critical state characterized by recurrent configurations, identifiable through the burning test [26].

Contrastingly, the toppling rule differs in the Abelian Manna model, which introduces an element of randomness. In this model, if  $z_i \geq 2$  at any site  $i$ , the site becomes

unstable and topples, reducing  $z_i$  to  $z_i - 2$ . The two grains are then distributed randomly and independently among nearest neighbors, with the possibility of selecting the same site twice:  $z_j \rightarrow z_j + 1$ . The remaining aspects of the Abelian Manna model mirror those of the BTW model described above.

### B. Eigen Microstates

In the sandpile system with  $N$  sites, we extract the states of the sites through simulations. By conducting measurements over  $M$  time steps, we obtain an  $N \times M$  matrix ( $M > N$ ) representing the state as  $S = (s_1, s_2, \dots, s_t, \dots, s_M)$ , where  $s_t = (s_{1t}, s_{2t}, \dots, s_{Nt})^T$  signifies the microstate of the system at time step  $t$ , and  $s_{it}$  is the number of topplings at site  $i$  during time step  $t$ . This matrix  $S$  can be treated as a statistical ensemble with dynamic microstates of the sandpile system. Utilizing

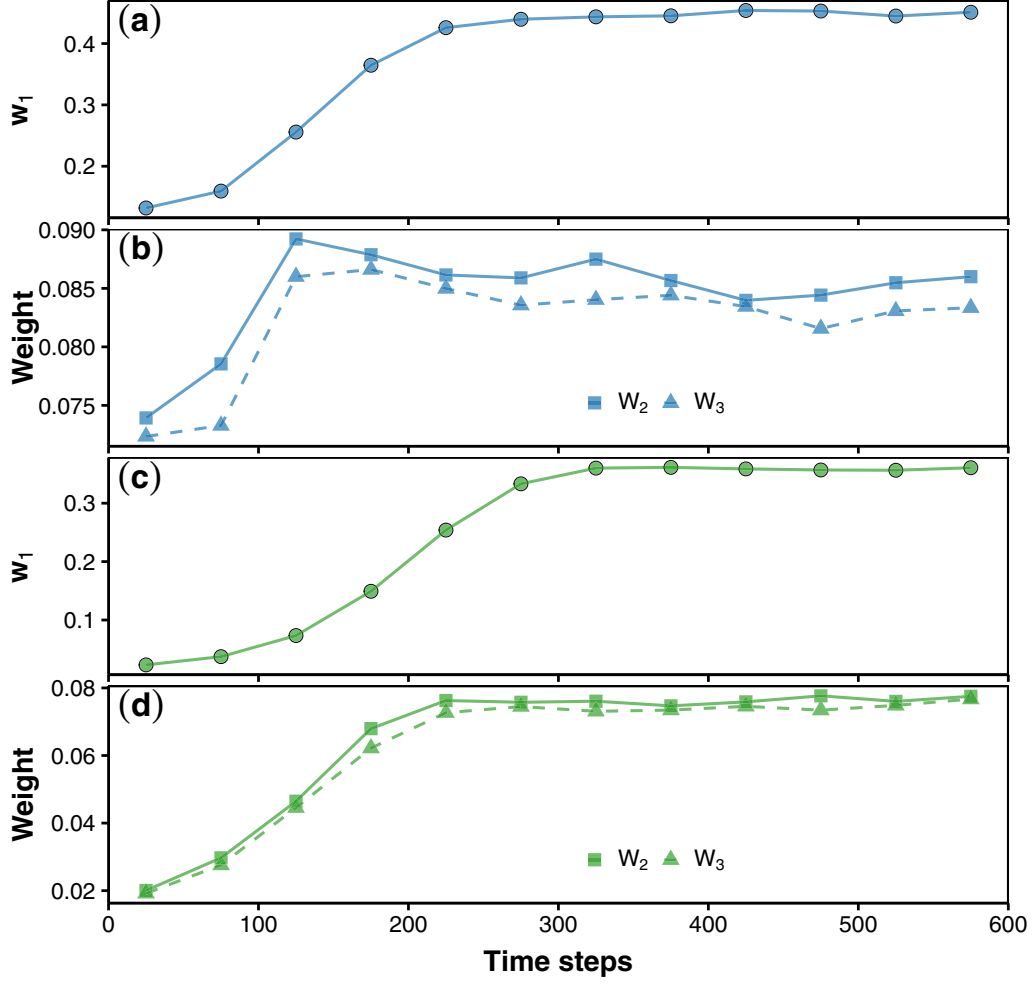


FIG. 2. Evolution of the weights: (a)  $w_1$  and (b)  $w_2$  and  $w_3$  of the eigenensemble from the absorbing state to the critical state for the BTW model with  $L = 32$ . (c) and (d) Similar to (a) and (b), but for the Manna model. Each ensemble matrix is calculated based on  $M = 5 \times 10^5$  from independent  $5 \times 10^5$  realizations.

singular value decomposition (SVD), we decompose the ensemble matrix as  $\mathbf{S} = \mathbf{U} \cdot \mathbf{\Lambda} \cdot \mathbf{V}^T$ , where  $\mathbf{\Lambda}$  is a  $N \times N$  diagonal matrix with nonzero eigenvalues  $\lambda_1 \geq \lambda_2 \geq \dots \geq \lambda_N \geq 0$ . The corresponding eigenvectors are represented by a  $M \times N$  unitary matrix  $\mathbf{V} = (\mathbf{v}_1, \mathbf{v}_2, \dots, \mathbf{v}_I, \dots, \mathbf{v}_N)$  and a  $N \times N$  unitary matrix  $\mathbf{U} = (\mathbf{u}_1, \mathbf{u}_2, \dots, \mathbf{u}_I, \dots, \mathbf{u}_N)$ , where  $\mathbf{v}_I = (v_{1I}, v_{2I}, \dots, v_{MI})^T$  and  $\mathbf{u}_I = (u_{1I}, u_{2I}, \dots, u_{NI})^T$ .

Furthermore, we express the ensemble matrix  $\mathbf{S}$  as [22]

$$\mathbf{S} = \sum_{I=1}^N w_I^{1/2} \mathbf{S}_I^E, \quad (1)$$

where  $\mathbf{S}_I^E$  is an  $N \times M$  eigenensemble matrix of the system with elements  $(\mathbf{S}_I^E)_{ii} = C_0^{1/2} u_{iI} v_{iI}$ . Here, the eigenvector  $\mathbf{u}_I$  corresponds to the normalized eigen microstates, and the eigenvector  $\mathbf{v}_I$  represents the normalized temporal eigen microstates. The constant amplitude is defined as  $C_0 = \sum_{I=1}^N \lambda_I^2 = \sum_{i=1}^M \sum_{I=1}^N s_{ii}^2$ , and  $w_I = \lambda_I^2 / \sum_{I=1}^N \lambda_I^2$  serves as a weight associated with the probability of the eigenensemble  $\mathbf{S}_I^E$  in the statistical ensemble  $\mathbf{S}$ . Further details regarding the eigen microstates approach can be found in Refs. [22–25].

For a given time step  $t$ , the avalanche size is denoted as  $A_s(t) = \sum_{i=1}^N s_{ii}$ . Consequently, the average avalanche size over  $M$  steps is expressed as

$$\langle A_s \rangle = \sigma_0^{1/2} \sum_{I=1}^N w_I^{1/2} \tilde{u}_I \tilde{v}_I, \quad (2)$$

where  $\sigma_0 = \frac{NC_0}{M}$ , and the parameters  $\tilde{u}_I$  and  $\tilde{v}_I$  are defined as

$$\tilde{u}_I = \frac{1}{\sqrt{N}} \sum_{i=1}^N u_{iI}, \quad (3)$$

$$\tilde{v}_I = \frac{1}{\sqrt{M}} \sum_{i=1}^M v_{iI}. \quad (4)$$

Given  $\sum_{I=1}^M v_{iI}^2 = 1$ , the second moment of the avalanche size is calculated as:

$$\langle A_s^2 \rangle = \sigma_0 \sum_{I=1}^N w_I \tilde{u}_I^2. \quad (5)$$

In our study, we employ  $L = 16, 32, 64, 96, 128$  and  $M = 5 \times 10^5$  to calculate the eigenensemble.

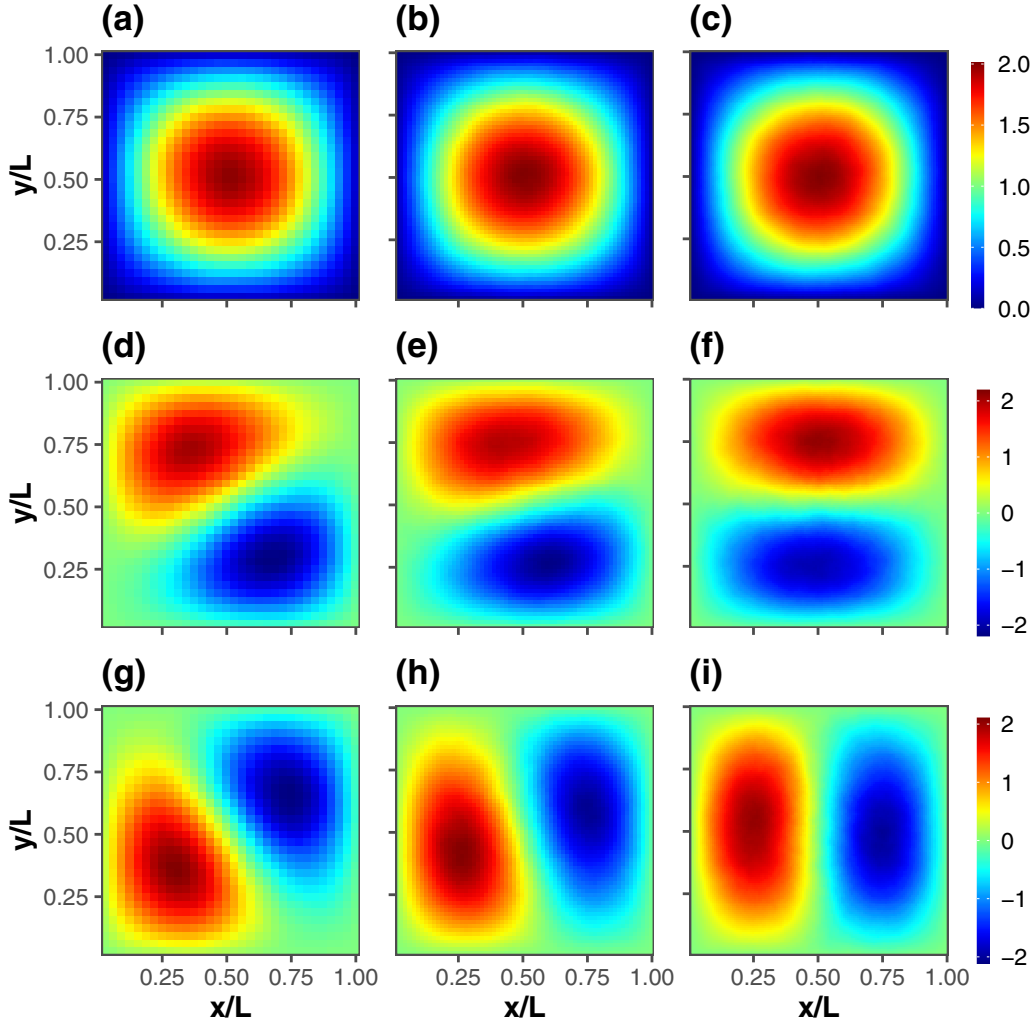


FIG. 3. Spatial distributions of the rescaled eigen microstates  $\mathbf{u}_i L$  for the BTW model at the critical state with different system sizes: (a)  $L = 32$ , (b)  $L = 64$ , and (c)  $L = 128$ . Correspondingly, (d)–(f) and (g)–(i) present the spatial distributions of  $\mathbf{u}_2 L$  and  $\mathbf{u}_3 L$  for the same system sizes, respectively.

### III. RESULTS

The simulations of the sandpile models, depicted in Fig. 1, illustrate the transition from the absorbing state to the critical state. In Figs. 1(a) and 1(b) (before the red dashed line), when the average height is low, the system resides in the absorbing state. Here, the average height increases proportionally with the addition of grains to the system. Subsequently, upon reaching the critical state, as evident in Figs. 1(a) and 1(b) (after the red dashed line), the average height stabilizes and fluctuates around a specific value. Throughout the critical state, the system's average energy remains constant for many time steps, indicative of a balance between energy input and dissipation. Both the BTW and Manna models exhibit a comparable evolution, albeit with distinct critical heights, as illustrated in Figs. 1(a) and 1(b).

An essential feature of SOC is its adherence to power-law behavior. The Probability Density Functions (PDFs) of avalanche sizes in subcritical and critical states are illustrated in Figs. 1(c) and 1(d). In the subcritical state, the distribution of  $A_s$  exhibits a faster decay as  $A_s$  increases

compared to the critical state. A proposed PDF satisfies  $P(A_s) = A_s^{-\tau_s} G(A_s/A_{sc})$ , where  $\tau_s$  represents a critical exponent, and  $G(x)$  is a scaling function. The cutoff for the system, denoted by  $A_{sc}$  ( $\sim L^D$ ), is determined by the system size, where  $D = 2.75$  is a critical exponent associated with the fractal dimension [27]. Beyond the avalanche size  $A_{sc}$ , the PDF experiences a rapid decay. In Figs. 1(c) and 1(d), we determine the exponents  $\tau_s = 1.10 \pm 0.07$  and  $1.17 \pm 0.04$  for the BTW model and the Manna model, respectively, with  $L = 32$ . A correction factor ( $\sim 1/\ln L$ ) can be applied to the critical exponent  $\tau_s$ . As  $L$  approaches infinity,  $\tau_s$  converges to 1.27 for both models [19,28].

We proceed to derive eigenensembles and their associated weights according to Eq. (1). The evolution of these weights, from the absorbing state to the critical state, is presented in Fig. 2. Notably, for both the BTW and Manna models, the dominant eigen microstate emerges, linked with the amplified weight  $w_1$ , as shown in Figs. 2(a) and 2(c). Upon reaching the critical state, the substantial weight  $w_1$  above 0.3 stabilizes, indicating the presence of a phase transition captured by

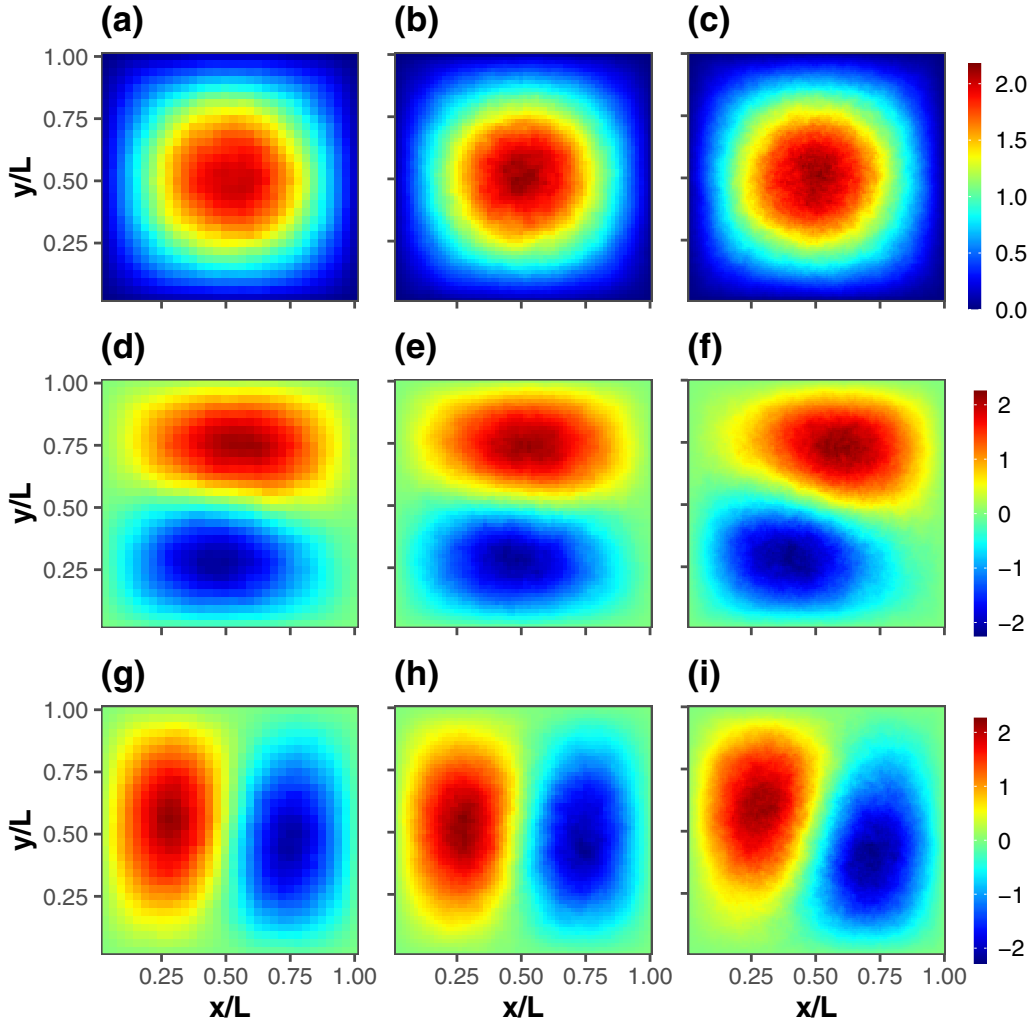


FIG. 4. Similar to Fig. 3, but for the Manna model.

the eigen microstates. It is akin to observations in the Ising model at the critical temperature [22].

Additionally, for the smaller weights  $w_2$  and  $w_3$  (almost degenerate), we observe an incremental increase as the system evolves toward the critical state, as demonstrated in Figs. 2(b) and 2(d). However, it is noteworthy that the maximum values of the weights  $w_2$  and  $w_3$  emerge earlier than that of  $w_1$ . This early emergence could potentially serve as an indicator for detecting early warning signals of the critical state for those systems that are not currently in a critical state but may be approaching one.

Spatial distributions of the rescaled eigen microstates  $\mathbf{u}_1L$ ,  $\mathbf{u}_2L$ , and  $\mathbf{u}_3L$  at the critical state are illustrated in Fig. 3 for the BTW model. The first eigen microstates reveals the universality and the presence of a giant cluster nearly matching the size of the system, with its components increasing from the boundary to the center of the system, as depicted in Figs. 3(a)–3(c).

The second-largest eigen microstates displays two clusters with opposite orientations, as seen in Figs. 3(d)–3(f). In order to maintain uniformity in the distribution, we have assigned positive values to the top area, considering that both  $\mathbf{u}_2$  and  $-\mathbf{u}_2$  can represent the second eigenvector. Given that

the eigenvectors are orthogonal, the third-largest eigen microstates will be rotated by  $\pi/2$  relative to the second-largest eigen microstates, as shown in Figs. 3(g)–3(i). These observed behaviors remain universal for different sizes. For the Manna model, the results closely mirror those of the BTW model in Fig. 4. Some differences are attributed to negligible random noise factors inherent in the Manna model.

We then explore the temporal eigen microstates  $\mathbf{v}_1$  at the critical state with varying system sizes. Figures 5(a) and 5(c) depict PDFs for the BTW model and the Manna model, respectively. Since all components of  $\mathbf{v}_1$  share the same sign (positive or negative), we enforce them to be positive. Three distinct regions emerge in the PDF of  $v_{i1}$ . For very small  $v_{i1}$ , the PDF remains unaffected by the increased  $v_{i1}$  in Figs. 5(a) and 5(c). In the medium range of  $v_{i1}$ , the PDF exhibits power-law decay with an exponent ( $\sim\tau_s$ ). Furthermore, for large  $v_{i1}$ , the PDF rapidly decays, influenced by the system size in Figs. 5(a) and 5(c).

Considering Eqs. (2) and (5), we can approximate  $\langle A_s \rangle \sim \sigma_0^{1/2} w_1^{1/2} \tilde{u}_1 \tilde{v}_1$  and  $\langle A_s^2 \rangle \sim \sigma_0 w_1 \tilde{u}_1^2$ , as the first eigen microstates is dominant. Consequently, we obtain  $\langle A_s \rangle^2 / \langle A_s^2 \rangle \sim \tilde{v}_1^2$ . For both the BTW model and the Manna model, the  $k$ th moment of the avalanche size follows  $\langle A_s^k \rangle \propto L^{D(1+k-\tau_s)}$

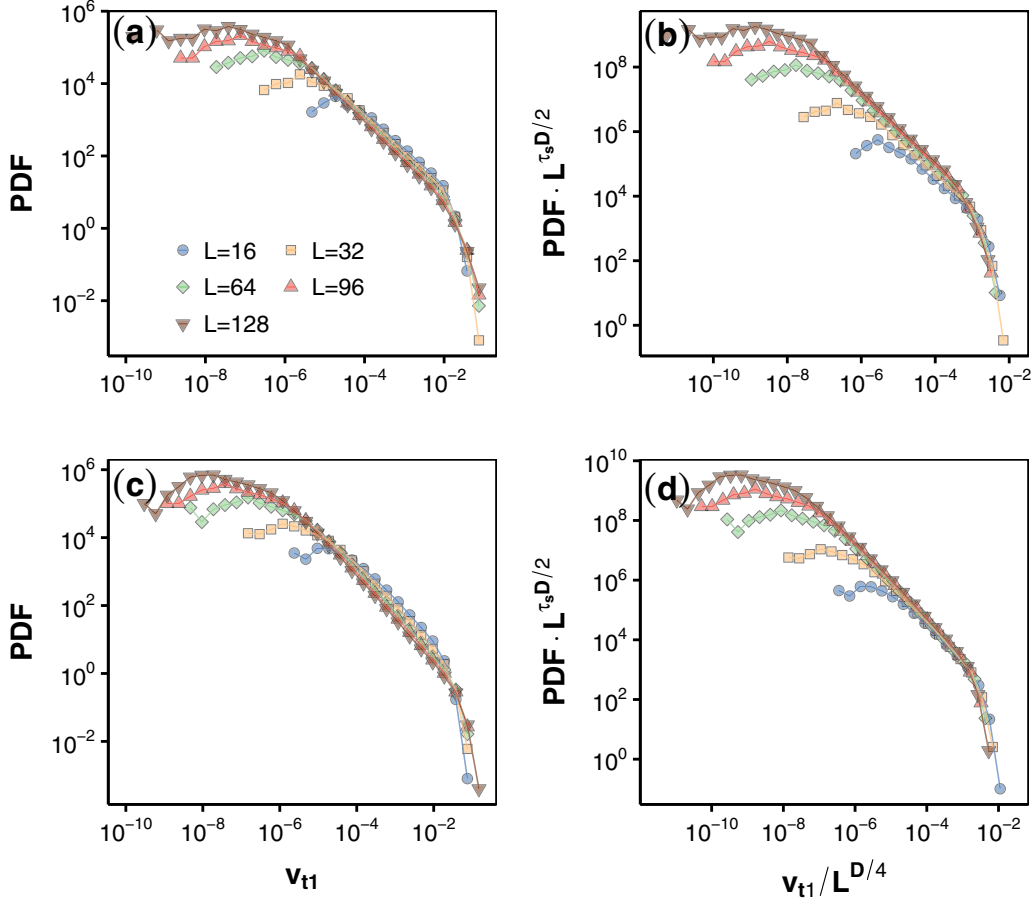


FIG. 5. PDFs of the components of the temporal eigen microstates  $v_{t1}$  for (a) the BTW model and (c) the Manna model at the critical state with various system sizes. Rescaled PDFs for (b) the BTW model and (d) the Manna model using the critical exponents  $\tau_s = 1.27$  and  $D = 2.75$ .

[1], resulting in  $\langle A_s \rangle^2 / \langle A_s^2 \rangle \propto L^{D(1-\tau_s)}$  and  $\tilde{v}_1 \propto L^{D(1-\tau_s)/2}$ . To establish the scaling relation, we have

$$\begin{aligned}
 \frac{1}{\sqrt{M}} \tilde{v}_1 &= \int_V v_{t1} PDF(v_{t1}; L) dv_{t1} \\
 &= \int_V v_{t1} L^{-\tau_s D/2} \mathcal{F}(v_{t1}/L^{D/4}) dv_{t1} \\
 &= \int_X (xL^{D/4}) L^{-\tau_s D/2} \mathcal{F}(x) L^{D/4} dx \\
 &= L^{D(1-\tau_s)/2} \int_X x \mathcal{F}(x) dx \quad (x = v_{t1}/L^{D/4}) \\
 &\propto L^{D(1-\tau_s)/2}. \tag{6}
 \end{aligned}$$

Based on Eq. (6), we rescale the PDF of  $v_{t1}$  with the critical exponents  $\tau_s = 1.27$  and  $D = 2.75$  in Figs. 5(b) and 5(d) for the BTW model and the Manna model, respectively. For the medium and large range of  $v_{t1}$ , the curves collapse across different system sizes. However, scaling breaks for very small  $v_{t1}$ . We speculate that the inherent fluctuation of the eigenvector related to the ratio  $N/M$  [29] rather than the critical behavior of the system influences the very small  $v_{t1}$ .

Next, we study the impact of system size on critical state parameters. The dependence of weight  $w_1$ ,  $\sigma_0$ , and  $\tilde{v}_1$  on system size is illustrated in Fig. 6. We observe  $w_1 \propto L^\alpha$  and

$\sigma_0 \propto L^\beta$  in Figs. 6(a) and 6(b), where  $\alpha$  and  $\beta$  are critical exponents detailed in Table I. Additionally, Fig. 6(c) demonstrates  $\tilde{v}_1 \propto L^{D(1-\tau_s)/2}$  with  $D(1-\tau_s)/2 = -0.31 \pm 0.01$  and  $-0.39 \pm 0.01$  for the BTW model and the Manna model, respectively.

By Eq. (2) and Eq. (5), we find  $\langle A_s^2 \rangle / \langle A_s \rangle \sim \sqrt{\sigma_0 w_1} \tilde{u}_1 / \tilde{v}_1$ . Since  $\tilde{u}_1$  remains constant with system size,

$$\sqrt{\sigma_0 w_1} / \tilde{v}_1 \propto L^D. \tag{7}$$

Figure 6(d) depicts the outcome, with the estimated critical exponent  $D$  presented in Table I. We also estimate the critical exponent  $\tau_s$  based on the results of Figs. 5(c) and 5(d), as indicated in Table I. The estimated critical exponents exhibit slight variations between the BTW model and the Manna model at the critical state. Notably, the estimated  $\tau_s$

TABLE I. Estimated critical exponents based on the first eigen microstates for both the BTW model and the Manna model at the critical state.

	$\alpha$	$\beta$	$D$	$\tau_s$
BTW	$0.12 \pm 0.01$	$4.27 \pm 0.05$	$2.50 \pm 0.03$	$1.25 \pm 0.05$
Manna	$0.09 \pm 0.01$	$4.50 \pm 0.03$	$2.69 \pm 0.02$	$1.29 \pm 0.03$

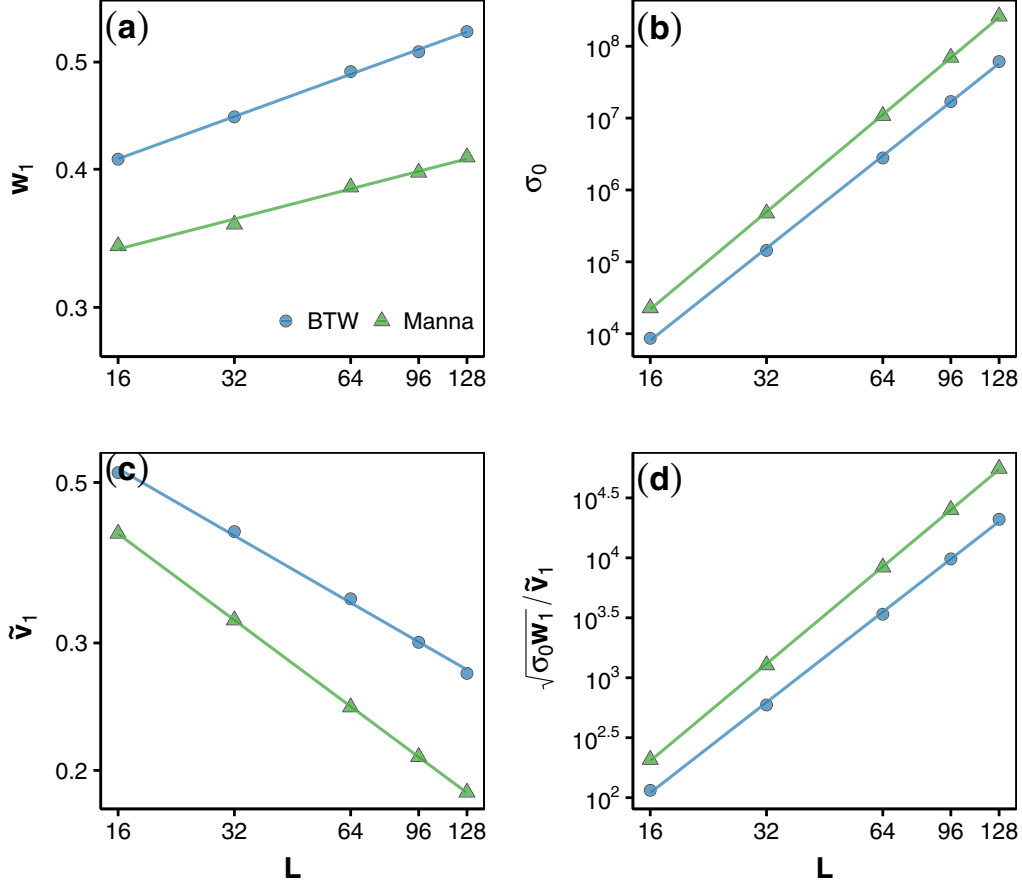


FIG. 6.  $\text{Log}_{10}\text{-log}_{10}$  plot of (a)  $w_1$ , (b)  $\sigma_0$ , (c)  $\tilde{v}_1$ , and (d)  $\sqrt{\sigma_0 w_1} / \tilde{v}_1$  as functions of the system size  $L$  for both the BTW model and the Manna model at the critical state. The fitted lines are presented.

derived from the first eigen microstates is closer to 1.27 than the estimated value from the PDF of avalanche size without corrections.

Alternatively, we can define the ensemble matrix as  $S^a$  with the element  $s_{it}^a$  representing the toppling area (multiple topples at the same site will only be counted once during a time step). Similarly, we obtain the eigenensemble and eigen microstates for the toppling area. Thus, the critical exponents  $D_a$  and  $\tau_a$  are estimated based on the first eigen microstates. For the toppling area, there is the same relation  $\langle A_a^k \rangle \propto L^{D_a(1+k-\tau_a)}$ . Regarding the parameter  $C_0^a$ , we have  $C_0^a = \sum_{t=1}^M \sum_{i=1}^N (s_{it}^a)^2 = \frac{1}{M} \langle A_a \rangle$  ( $s_{it}^a$  can only be one or zero), implying that  $\sigma_0^a \propto L^{D_a(2-\tau_a)+2}$ . Therefore, we deduce the relation  $w_1^a L^2 \propto L^{D_a}$  from Eq. (7).

Figure 7(a) displays the results. The critical exponents  $D_a = 2.05 \pm 0.01$  and  $2.04 \pm 0.01$  are estimated for the BTW model and the Manna model, respectively, both closely approaching two since avalanches in two dimensions are compact [27]. Thus, the critical exponent  $\gamma_{sa} = D/D_a$  between the toppling number and area is  $1.22 \pm 0.04$  and  $1.32 \pm 0.03$  for the BTW model and the Manna model, respectively. Previous studies suggested that both  $\gamma_{sa}$  for the two models are around 1.35 or even smaller for BTW [19,20]. Based on the dependence of  $\tilde{v}_1^a$  on the system size in Fig. 7(a), we can estimate the critical exponent  $\tau_a = 1.18 \pm 0.01$  and  $1.32 \pm 0.01$

for the BTW model and the Manna model, respectively. The obtained exponent is smaller for the BTW model, with its exact value suggested to be  $4/3$  [28].

#### IV. CONCLUSIONS

In conclusion, our investigation into the eigen microstates of SOC through the study of sandpile models, particularly the BTW and Manna models, has revealed intriguing findings. We observed the emergence of dominant eigen microstates associated with amplified weights as these systems transitioned from an absorbing state to a critical state. This behavior mirrors the phase transition phenomena observed in other critical systems, such as the Ising model. Notably, the non-dominant weights, specifically  $w_2$  and  $w_3$ , unveil themselves as potential indicators for detecting early warning signals of the critical state.

Spatial analyses of normalized eigen microstates divulge avalanche characteristics across various spatial scales, from the entire system down to half scale or smaller. The examination of PDFs for the components of the temporal eigen microstates  $v_1$  imparts critical behavioral insights. The establishment of scaling relations, coupled with rescaled PDFs, demonstrate collapse for medium and large  $v_1$  values.

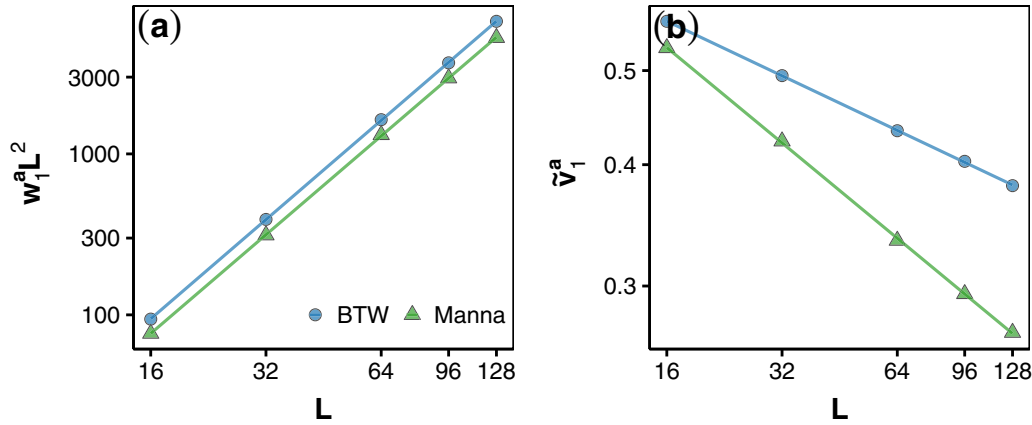


FIG. 7.  $\text{Log}_{10}\text{-log}_{10}$  plot of (a)  $w_1^a L^2$  and (b)  $v_1^a$  as functions of the system size  $L$  for both the BTW model and the Manna model at the critical state. The fitted lines are presented.

Moreover, we introduced an analysis of finite size effects on the first eigen microstates to estimate critical exponents for both the BTW and Manna models at the critical state, i.e.,  $\sqrt{\sigma_0 w_1}/\tilde{v}_1 \propto L^D$  and  $\tilde{v}_1 \propto L^{D(1-\tau_s)/2}$ . Our investigation extended further to the toppling area, where the critical exponent  $\gamma_{sa} = D/D_a$  between the toppling number and area revealed values of  $1.22 \pm 0.04$  and  $1.32 \pm 0.03$  for the BTW and Manna models, respectively.

#### ACKNOWLEDGMENTS

We thank the National Natural Science Foundation of China (Grants No. 12305044 and No. 12135003) and the National Key Research and Development Program of China (Grant No. 2023YFE0109000) for financial support. G.H. acknowledges financial support from the China Postdoctoral Science Foundation (Grant No. 2023M730299).

- [1] K. Christensen and N. R. Moloney, *Complexity and Criticality* (Imperial College Press, London, 2005).
- [2] P. Bak, C. Tang, and K. Wiesenfeld, Self-organized criticality: An explanation of the  $1/f$  noise, *Phys. Rev. Lett.* **59**, 381 (1987).
- [3] B. Gutenberg and C. F. Richter, Frequency of earthquakes in California, *Bull. Seismol. Soc. Am.* **34**, 185 (1944).
- [4] O. Peters and J. D. Neelin, Critical phenomena in atmospheric precipitation, *Nat. Phys.* **2**, 393 (2006).
- [5] P. Bak, K. Christensen, L. Danon, and T. Scanlon, Unified scaling law for earthquakes, *Phys. Rev. Lett.* **88**, 178501 (2002).
- [6] R. Sánchez, D. E. Newman, and B. A. Carreras, Waiting time statistics of self-organized-criticality systems, *Phys. Rev. Lett.* **88**, 068302 (2002).
- [7] M. Paczuski, S. Boettcher, and M. Baiesi, Interoccurrence times in the Bak-Tang-Wiesenfeld sandpile model: A comparison with the observed statistics of solar flares, *Phys. Rev. Lett.* **95**, 181102 (2005).
- [8] A. Deluca, N. R. Moloney, and Á. Corral, Data-driven prediction of thresholded time series of rainfall and self-organized criticality models, *Phys. Rev. E* **91**, 052808 (2015).
- [9] S. S. Manna, Sandpile models of self-organized criticality, *Curr. Sci.* **77**, 388 (1999).
- [10] R. Dickman, A. Vespignani, and S. Zapperi, Self-organized criticality as an absorbing-state phase transition, *Phys. Rev. E* **57**, 5095 (1998).
- [11] A. Vespignani, R. Dickman, M. A. Muñoz, and S. Zapperi, Driving, conservation, and absorbing states in sandpiles, *Phys. Rev. Lett.* **81**, 5676 (1998).
- [12] A. Vespignani, R. Dickman, M. A. Muñoz, and S. Zapperi, Absorbing-state phase transitions in fixed-energy sandpiles, *Phys. Rev. E* **62**, 4564 (2000).
- [13] S. S. Manna, Two-state model of self-organized criticality, *J. Phys. A: Math. Gen.* **24**, L363 (1991).
- [14] D. Dhar, The Abelian sandpile and related models, *Physica A* **263**, 4 (1999).
- [15] Y.-C. Zhang, Scaling theory of self-organized criticality, *Phys. Rev. Lett.* **63**, 470 (1989).
- [16] V. Frette, K. Christensen, A. Malthe-Sørensen, J. Feder, T. Jøssang, and P. Meakin, Avalanche dynamics in a pile of rice, *Nature (London)* **379**, 49 (1996).
- [17] K. Christensen, Á. Corral, V. Frette, J. Feder, and T. Jøssang, Tracer dispersion in a self-organized critical system, *Phys. Rev. Lett.* **77**, 107 (1996).
- [18] L. Pietronero, A. Vespignani, and S. Zapperi, Renormalization scheme for self-organized criticality in sandpile models, *Phys. Rev. Lett.* **72**, 1690 (1994).
- [19] A. Chessa, H. E. Stanley, A. Vespignani, and S. Zapperi, Universality in sandpiles, *Phys. Rev. E* **59**, R12 (1999).
- [20] A. Ben-Hur and O. Biham, Universality in sandpile models, *Phys. Rev. E* **53**, R1317 (1996).
- [21] E. Milshtein, O. Biham, and S. Solomon, Universality classes in isotropic, Abelian, and non-Abelian sandpile models, *Phys. Rev. E* **58**, 303 (1998).
- [22] G. Hu, T. Liu, M. Liu, W. Chen, and X. Chen, Condensation of eigen microstate in statistical ensemble and phase transition, *Sci. China Phys. Mech. Astron.* **62**, 990511 (2019).

- [23] Y. Sun, G. Hu, Y. Zhang, B. Lu, Z. Lu, J. Fan, X. Li, Q. Deng, and X. Chen, Eigen microstates and their evolutions in complex systems, *Commun. Theor. Phys.* **73**, 065603 (2021).
- [24] T. Liu, G. Hu, J. Dong, J. Fan, M. Liu, and X. Chen, Renormalization group theory of eigen microstates, *Chinese Phys. Lett.* **39**, 080503 (2022).
- [25] X. Li, T. Xue, Y. Sun, J. Fan, H. Li, M. Liu, Z. Han, Z. Di, and X. Chen, Discontinuous and continuous transitions of collective behaviors in living systems, *Chinese Phys. B* **30**, 128703 (2021).
- [26] D. Dhar, Studying self-organized criticality with exactly solved models, [arXiv:cond-mat/9909009](https://arxiv.org/abs/cond-mat/9909009).
- [27] C. Tebaldi, M. De Menech, and A. L. Stella, Multifractal scaling in the Bak-Tang-Wiesenfeld sandpile and edge events, *Phys. Rev. Lett.* **83**, 3952 (1999).
- [28] S. Lübeck and K. D. Usadel, Numerical determination of the avalanche exponents of the Bak-Tang-Wiesenfeld model, *Phys. Rev. E* **55**, 4095 (1997).
- [29] J. Bun, J.-P. Bouchaud, and M. Potters, Cleaning large correlation matrices: Tools from random matrix theory, *Phys. Rep.* **666**, 1 (2017).